ELSEVIER

Journal of Nuclear Materials 257 (1998) 67–77

journal of nuclear materials

# Oxidation kinetics of Zircaloy-2 between 450°C and 600°C in oxidizing atmosphere

T. Arima *, K. Moriyama, N. Gaja, H. Furuya, K. Idemitsu, Y. Inagaki

*Department of Nuclear Engineering, Kyushu University, 6-10-1 Hakozaki, Fukuoka 812 8581, Japan*

Received 13 October 1997; accepted 16 April 1998

**Abstract**

The oxidation kinetics of Zircaloy-2 have been studied in the temperature range 450–600°C under the atmosphere of flowing Ar/5%$H_2$, $CO_2$/1%CO, and $CO_2$. Using the micro-balance technique, the weight change of the specimen has been measured as a function of time. The results showed that the oxidation kinetics of Zircaloy-2 obeyed the cubic rate law rather than the parabolic one. The effect of oxygen partial pressure on the rate constant was not found under the present experimental conditions. On the other hand, the activation energies of the oxidation were 145, 171, and 188 kJ/mol for Ar/5%$H_2$, $CO_2$/1%CO, and $CO_2$ atmospheres, respectively. It was shown from the X-ray diffractometry that the specimens oxidized under the conditions of this study consisted mainly of monoclinic zirconia and, to a minor degree, of tetragonal one. It is suggested that the lateral cracks observed with scanning electron microscopy (SEM) may cause the slow diffusion of oxygen in the oxide phase. 

*PACS:* 28.41.T; 81.65.M

## 1. Introduction

Zircaloy has been used as a cladding material for light water reactors (LWR). Recently, it is planned that the burn-up of the fuel of LWR is to be extended up to over 50 GWd/t and (U, Pu)$O_2$ fuel (MOX) be used as fuel for LWR. Under these new conditions, oxygen potentials ($\Delta\overline{G}_{O_2} = RT \ln p_{O_2}$) at the fuel–cladding gap may be expected to increase. Part of released oxygen will be combined with fission products, while the others should be accumulated to increase the O/M ratio of the fuel leading to increase in the oxygen potential at the fuel–cladding gap.

The oxidation of cladding materials is one of the modes of the fuel–cladding chemical interaction (FCCI). Since the free energy of formation of zirconium oxide is very low ($<\sim -900$ kJ/mol) [1], zirconium metal easily combines with oxygen and becomes the oxide, resulting in thinning of the cladding. In addition, the oxygen potential at the fuel–cladding gap affects the chemical behavior of the fission products such as Cs or Te, which can accelerate corrosion of the cladding. Then importance of study on zircaloy oxidation in wide ranges of oxygen pressure and temperature should be emphasized in relation with the irradiation performance and safety of fuel pins.

The corrosion behavior of zirconium alloys as cladding-materials have been so far discussed for many years [2]. A number of papers have been published on the water side corrosion, but not so many studies have been done on the corrosion of cladding inner surface. And it is known that the oxidation kinetics obey the parabolic or cubic rate law preceding the linear one. Westerman [3] and Dawson et al. [4] reported the insensitivity of pre-transition oxidation to oxygen pressure. Nakamura showed that the dependency of oxidation rate on oxygen partial pressure is very weak in the cubic rate law region [5]. The investigated ranges of the oxygen partial pressure (above approx. $2 \times 10^{-4}$ atm) were found to be higher than those predicted from the fuel–cladding gap [6]. The predicted values are considered to be above $10^{-68}$–$10^{-38}$ atm, which are in-

* Corresponding author. Tel.: +81-92 642 3779; fax: +81-92 642 3800; e-mail: arimatne@mbox.nc.kyushu-u.ac.jp.

0022-3115/98/$ – see front matter 
PII: S0022-3115(98)00069-5

Table 1
Chemical composition of Zircaloy-2

| Element | Sn | Fe | Cr | Ni | O | Zr |
|---|---|---|---|---|---|---|
| wt% | 1.5 | 0.17 | 0.12 | 0.07 | 0.13 | bal. |

fluenced by many factors (e.g. cladding temperature, burn-up, and fission products coexisting at the fuel–cladding gap).

Therefore, in this study, the dependence of the oxidation rate of Zircaloy-2 on both the oxygen partial pressure ($10^{-30}$–$10^{-2}$ atm) and temperature (450–600°C) has been measured for the oxidation time of 24 h using the micro-balance technique. On the basis of obtained data and observation of the oxide layer with X-ray diffraction (XRD) and scanning electron microscopy (SEM), the oxidation behavior of Zircaloy-2 has been discussed.

## 2. Experimental

The specimens of Zircaloy-2 studied in this experiment were cut from the α-forged rod, and were prepared into the form of a disk which has the geometry of 4 mm diameter and approximately 0.5 mm thickness. The chemical analyses of the specimen are listed in Table 1. The specimen surface was polished on abrasive papers and then subsequently finished by alumina buffing.

The oxidation experiment has been carried out using a micro-balance apparatus (Cahn-2000). The schematic diagram of the micro-balance and associated gas supplying system is shown in Fig. 1.

The desired oxygen potential or oxygen partial pressure was obtained by changing the composition of the flowing gas components, i.e., Ar/5%$H_2$, $CO_2$/1%CO, and $CO_2$. These gases were supplied at a constant flow rate under the atmospheric pressure. The oxygen partial pressures were measured at downstream of the heating furnace by a calcia stabilized zirconia (CSZ) oxygen sensor.

With regard to the measurement of the oxygen potential, a little inconsistency was found between the measured oxygen potential value and the theoretical one calculated on the basis of chemical equilibrium except the atmosphere of Ar/5%$H_2$. The former was larger than the latter in each case. These results cannot be explained with the experimental error, which was estimated to be ±15% by a calibration test described later. This inconsistency seems to arise from the reason that uncontrollable impurity gas and moisture contaminated the atmospheric gas in the furnace. This is because this oxygen sensor was calibrated in the air|CSZ|depressed–air system and showed a good linearity between the controlled oxygen potential and the measured electrical potential. Therefore the authors assumed that the values measured by the CSZ were more correct. Thus the oxygen pressures, which corresponded to measured electrical potentials, of Ar/5%$H_2$, $CO_2$/1%CO, and $CO_2$ were obtained to be $1.5 \times 10^{-30}$–$2.9 \times 10^{-25}$, $8.8 \times 10^{-18}$–$8.0 \times 10^{-17}$, and $4.9 \times 10^{-3}$–$2.3 \times 10^{-2}$ atm, respectively.

Before the isothermal oxidation experiment was performed, the oxidation furnace was kept at room

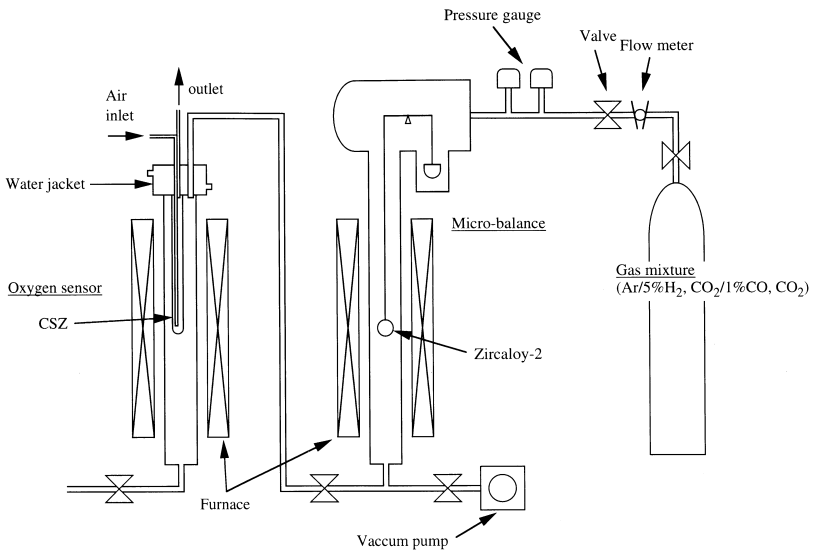


Fig. 1. Schematic diagram of the oxidation apparatus. It consists of micro-balance, oxygen sensor, and associated gas supplying equipment.

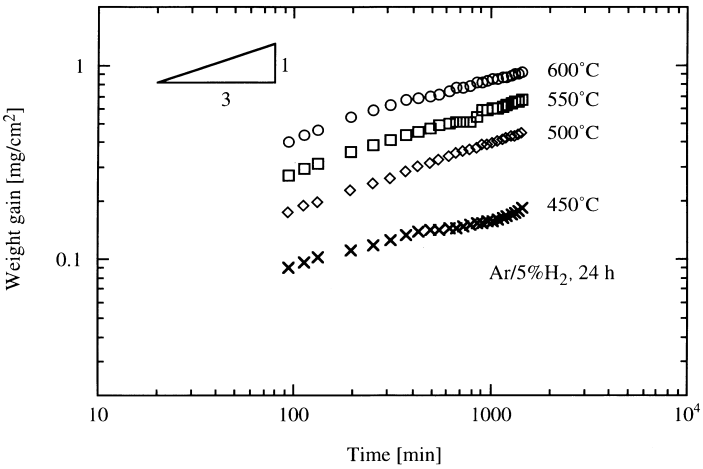


Fig. 2. The weight gain curves in Ar/5%$H_2$ gas mixture for Zircaloy-2. The continuous weight change is measured with the micro-balance in the temperature range 450–600°C.

temperature for over 8 h under the condition that the specimen was hanging and the gas was flowing, in order to stabilize the micro-balance and the CSZ oxygen sensor. Then, the temperature of the oxidation furnace was quickly raised up to the desired value. After that, it was isothermally kept constant within an error of ±0.5°C. The oxidation experiments were performed at 450°C, 500°C, 550°C, and 600°C each.

For the observation of microstructure, the sections were cut from the specimens, and were embedded in the Cu-based resin, which has an electric conductivity. The embedded sections were prepared as the specimens for SEM examination. The cross sections of these specimens were mechanically polished as described above, then chemically polished using a swabbing-technique with a solution of 10 vol.% HF, 45 vol.% $HNO_3$, and 45 vol.%$H_2O$.

In order to identify the surface oxide layer, X-ray pattern was taken on the specimen surface using an XD-D1 Shimadzu diffractometer. The diffracrometer was used with Cu Kα radiation and at conditions of 30 keV and 30 mA. Since the thickness of the oxide layer was considered to be thin, the diffraction patterns were measured with the small X-ray incident angle ($\theta_{\text{incident}} = 1°$), which is fixed for oxidized specimens. It was, therefore, found that the diffraction intensity from the surface oxide layer was strongly diffracted without being obscured by the X-ray diffracted from the internal matrix metal.

## 3. Results

### 3.1. Oxidation kinetics

The continuous change in the weight of specimen was measured as a function of time with the micro-balance. The weight gains per unit area under the atmosphere of

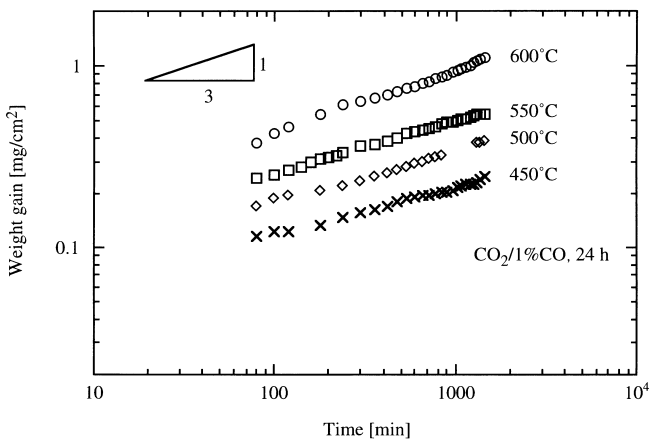


Fig. 3. The weight gain curves in $CO_2$/1%CO gas mixture.

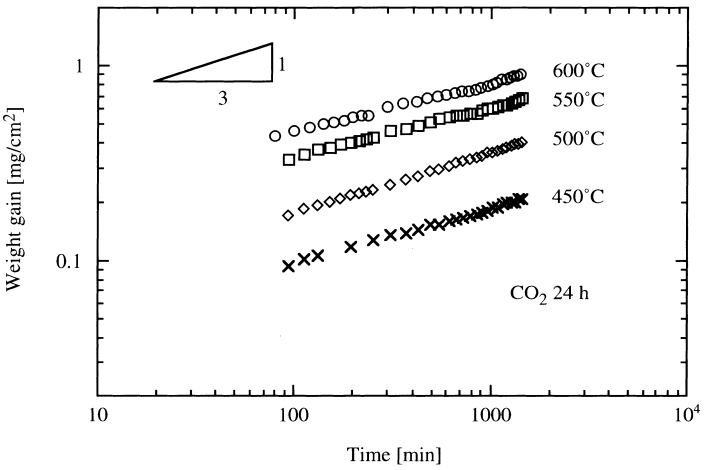


Fig. 4. The weight gain curves in $CO_2$ gas mixture.

either Ar/5%$H_2$, $CO_2$/1%CO, or $CO_2$ are shown in Figs. 2–4, respectively. In these figures, both axes of ordinate and abscissa are expressed in logarithm, in order to compare the results with other researchers' results. The weight gains in all curves increase smoothly with time which means no occurrence of kinetic transition during the oxidation experiment. As shown in Figs. 2–4, the slopes of weight gain curves approximate to 1/3 and this result shows that the cubic rate law is preferable to parabolic one for the oxidation kinetics of Zircaloy-2.

### 3.2. XRD examination

Fig. 5(a)–(d) shows the X-ray diffraction patterns of as-received Zircaloy-2 and the specimens heated under the conditions of $CO_2$ at 450°C, $CO_2$ at 600°C, and Ar/5%$H_2$ at 600°C, respectively. The diffraction pattern from Zircaloy-2 sample, which was not oxidized, was measured by using normal $2\theta$–$\theta$ method. Other peak patterns from the specimens heated for 24 h were measured by using the low incident angle-parallel beam method mentioned above. As a result, the peak patterns from zirconium oxides could be observed without hallow peaks from matrix material (Zircaloy-2). Most peak intensities from oxidized samples originated from monoclinic $ZrO_2$. The small peak intensities at $2\theta = \sim 30°$ may indicate existence of tetragonal $ZrO_2$. Peak patterns from the other forms of zirconium oxide, i.e., orthorhombic or cubic, were not found. Such a tendency was not affected by the oxidation temperature and atmosphere.

### 3.3. SEM examination

Fig. 6(a)–(c) shows the SEM photographs of oxide formed on the specimens heated under the conditions of $CO_2$ at 450°C, $CO_2$ at 600°C, and Ar/5%$H_2$ at 600°C, respectively. In $CO_2$ atmosphere, the oxide layer on the specimen oxidized at 600°C (5–6 μm) is thicker than the one at 450°C (1–2 μm). From observation of the oxide thickness it was found to be almost proportional to the

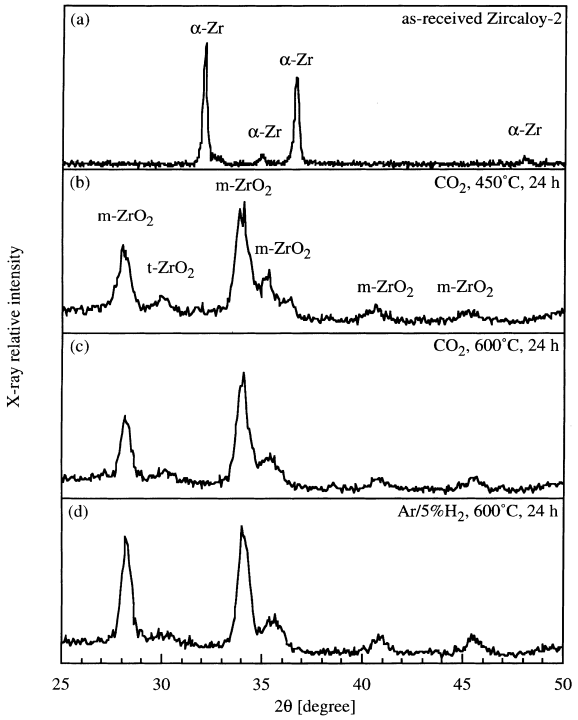


Fig. 5. X-Ray diffraction patterns of: (a) as-received Zircaloy-2, specimens oxidized; (b) in $CO_2$ at 450°C; (c) in $CO_2$ at 600°C; (d) in Ar/5%$H_2$ at 600°C (α: hexagonal, m: monoclinic, t: tetragonal). The diffraction patterns of oxidized specimens were measured by using the low incident angle-parallel beam method with $\theta_{incident} = 1°$.

weight gain of the specimens. The relation between the oxide thickness and the weight gain is often expressed as a following convenient formula, 1.5 mg/dm$^2$ = 100 nm. The results are found to hold good in this relationship. The difference in the oxide layer due to the atmosphere, where each atmosphere has different gas components and oxygen potential, could not be observed. In Fig. 6(b) and (c), we noticed two common characters of the thick oxide layers. One is that an interface shape between the oxide layer and the matrix (metal) is wavy rather than flat, and the other is that the lateral cracks, which are parallel to the surface of the specimen, are distributed near the interface within the oxide layer. Part of oxide layer under the detected cracks seems to be thin. This result shows that these cracks prevent the oxide layer from growing into the metal.

## 4. Discussions

Generally, the weight gain due to the oxidation can be expressed as the inverse power $n$ of oxidation time, as shown by the following equation:

$$W_0 = k_1 + k_2 \cdot t^{1/n}, \tag{1}$$

where $W_0$ is the apparent weight gain, $k_1$ and $k_2$ are the proportional constants. $n$ equals to 2 for the parabolic and 3 for the cubic behavior. Using above equation, we performed the $\chi^2$ test. When $k_1$ and $k_2$ are independent on each other, the $\chi^2_{\text{cubic}}$ values are smaller than $\chi^2_{\text{parabolic}}$ ones for 10 cases among 12 experimental conditions. If $k_1$ is fixed as zero and only $k_2$ is free, then the $\chi^2_{\text{cubic}}$ values are smaller for all cases. From this test, our result prefers the cubic rate law to the parabolic one.

If an isothermal experiment is ideally carried out, $k_1$ is considered to be zero. But in practice $k_1$ is often found

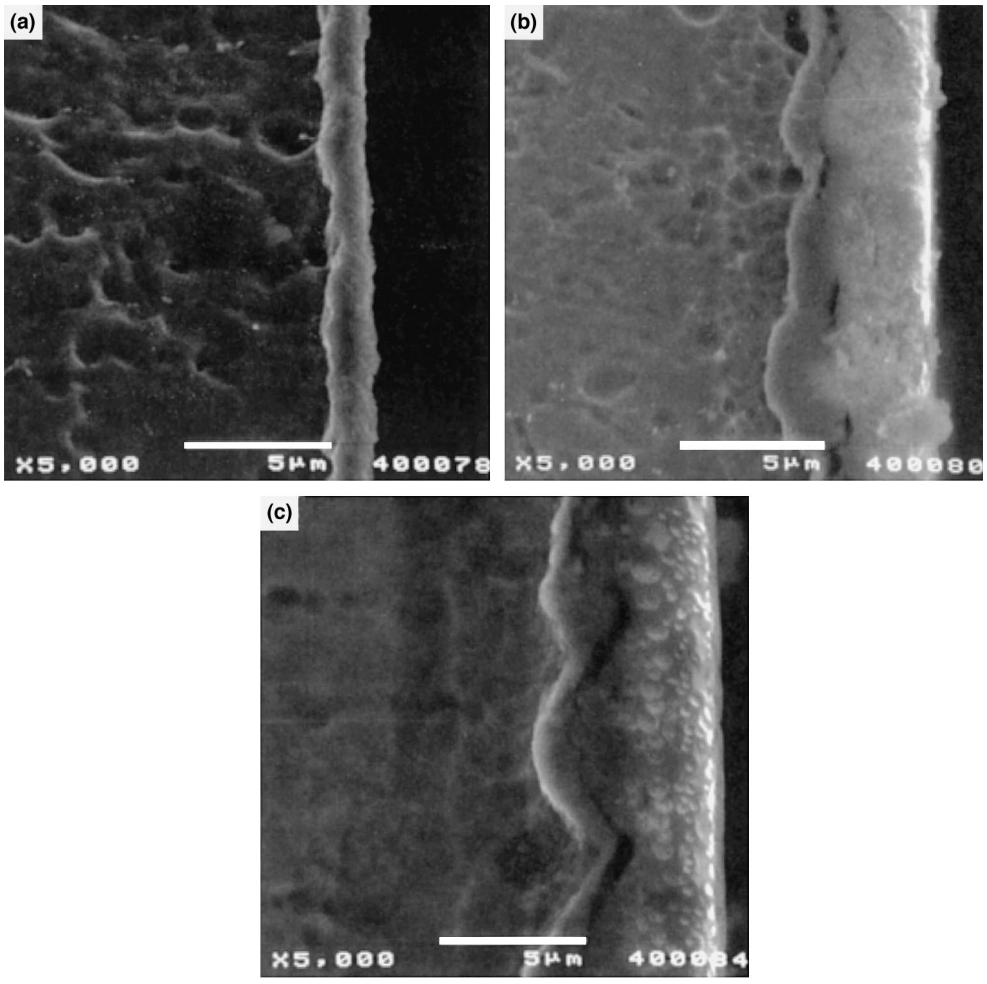


Fig. 6. The SEM photographs of oxide formed on Zircaloy-2: (a) in $CO_2$ at 450°C; (b) $CO_2$ at 600°C; (c) Ar/5%$H_2$ at 600°C.

not to be zero. It may be mainly caused by buoyancy and heat convection. An apparent weight gain due to buoyancy can be estimated by the following formula:

$$\frac{m_b}{S} = 273\,\rho_{273} V\left(\frac{1}{300} - \frac{1}{T}\right)\frac{1}{S}, \tag{2}$$

where $m_b$ is buoyancy when the temperature is raised from 300 to $T$ K, $\rho_{273}$ is the gas density at 273 K, $V$ and $S$ are the volume and the surface area of the specimen [7]. It increases with the temperature and is estimated to be less than 0.03 mg/cm$^2$ for every atmosphere at 873 K. The results from the blank tests which involve both effects, buoyancy and heat convection, show that the apparent weight gain is not more than 0.05 mg/cm$^2$ and are consistent with the values of $k_1$ derived by applying the cubic rate law rather than the parabolic one. In general, the cubic rate law is defined as

$$W^3 = k_c t, \tag{3}$$

where $k_c$ is the cubic rate constant. Complying with this definition, the $k_2^3$ is the cubic rate constant $k_c$.

The effect of the oxygen partial pressure on the oxidation kinetics is shown in Fig. 7. The data are a little scattered, but it seems that the cubic rate constant is independent of the oxygen partial pressure. Similarly, in other experiments, the oxygen partial pressure dependence of the rate constant cannot be seen in the pre-transition stage under the dry condition with the oxygen partial pressure of more than $10^{-4}$ atm [3–5,8,9]. Whereas, under the wet condition or in the post-transition stage of the dry condition, the oxidation rate constant seems to increase with the water vapor pressure and the oxygen partial pressure, respectively [3,5]. Poulton and Smeltzer [10] reported that the self-diffusion coefficient in m-$ZrO_2$ was independent of oxygen pressure in the range $10^{-19}$–1 atm. The values of the rate constants as well as their dependency on the oxygen partial pressure obtained in this study are compatible with other experimental results.

If the rate control process of the oxidation kinetics is caused by the vacancy diffusion through the anion site in the oxide film, the effect of the oxygen pressure cannot appear on the oxidation kinetics, which have been pointed out by Beie et al. [11] as follows. The rate constant can be given by

$$k \propto \left[\left(\frac{1}{p'_{O_2}}\right)^{1/6} - \left(\frac{1}{p''_{O_2}}\right)^{1/6}\right], \tag{4}$$

where $p'_{O_2}$ is the oxygen partial pressure at the equilibrium given by $ZrO_2 = Zr + O_2$ and $p''_{O_2}$ is that of the environmental gas. It is assumed here that the oxygen vacancies are generated by the reaction, $O_o = V_o^{\cdot\cdot} + 2e^- + \frac{1}{2}O_2$, where $O_o$, $V_o^{\cdot\cdot}$, and $e^-$ are an oxygen atom at its regular site, a doubly charged oxygen vacancy, and electron, respectively. Even for the lowest oxygen partial pressure used this study, $p''_{O_2}$ is much larger than $p'_{O_2}$ (e.g. $\sim 10^{-70}$ atm at 450°C) and then $k$ is almost independent on $p''_{O_2}$. In other words, it means that the growing zirconia has the character of n-type semi-

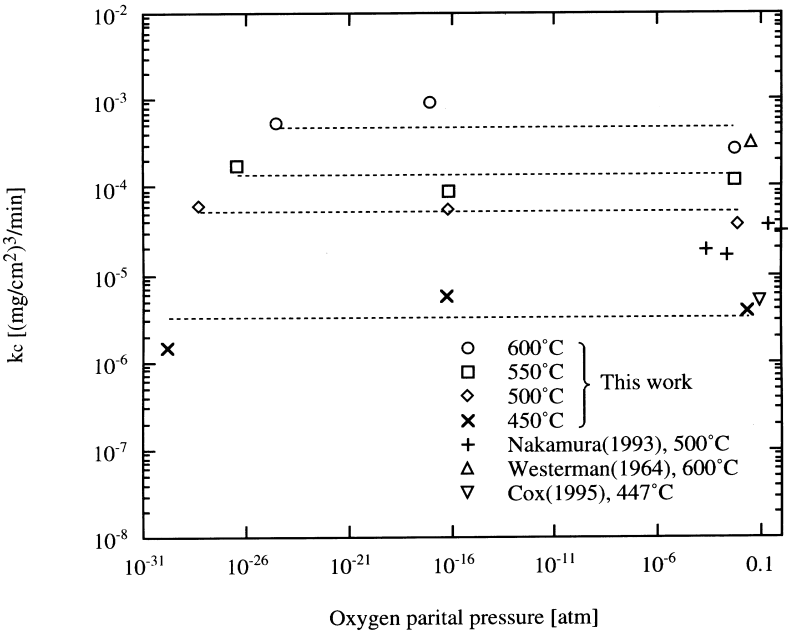


Fig. 7. The effect of the oxygen partial pressure on the cubic rate constant. The rate constants of the other oxidation experiments are derived from each figure in Refs. [3,5,8].

conductor [11]. In addition, it is known that the oxygen deficient zirconia has a black, whereas the zirconia with ideal composition has a white color. In this experiment, all specimens showed black zirconia films. It is, therefore, suggested that the growing oxide film on the metal is the oxygen deficient zirconia and the oxygen kinetics are controlled by the anion vacancy diffusion. The performance observed in this study supports the independence of the $k$ on the oxygen partial pressure.

The temperature dependence of the rate constant is generally written as

$$k_c = A \exp\left(-\frac{Q}{RT}\right), \tag{5}$$

where $A$ is a constant, $R$ is a gas constant, $T$ is the temperature, and Q is the activation energy. The cubic rate constants are shown as the function of $1/T$ in Fig. 8. The activation energy for each atmospheric condition can be obtained by the least squares fitting with Eq. (5) and is listed in Table 2. It seems that the activation energy increases with the oxygen partial pressure. But this tendency may be attributed to the experimental error. In Fig. 9, the cubic rate constants thus obtained are shown with other experimental results. Irrespective of the difference among the atmospheric conditions, the activation energy is a little greater at high temperature region than at low temperature region. For high temperature region over 600°C, the activation energy was 215 kJ/mol by Westerman [3]. On the other hand, that for the low temperature region of less than 400°C was found to be

Table 2
Activation energy obtained in pre-transition region

| Gas mixture | $Ar/5\%H_2$ | $CO_2/1\%CO$ | $CO_2$ |
|---|---|---|---|
| Activation energy (kJ/mol) | 145 | 171 | 188 |

130 kJ/mol by Hillner [2]. The activation energies obtained here were distributed between these values. In addition, Cox and Pemsler reported that the activation energies for the lattice diffusion process and the non-lattice process, e.g., grain boundaries, impurity, or dislocation, were found to be approximately 240 kJ/mol and 130–140 kJ/mol, respectively [12]. As a result, it seems that the oxidation kinetics was influenced by the lattice diffusion process at the high temperature region. While, at low temperature region, the non-lattice diffusion process, which the vacancy concentration is determined by the extrinsic factors, may control the oxidation kinetics. Thus the non-lattice diffusion process can be expected to have the small activation energy and little dependence of oxygen partial pressure on the rate constant.

In the oxidation kinetics of the metal, the dissolution of the oxygen atoms into the metal under the growing oxide must be taken into consideration. Total amount of the oxygen dissolved per unit area in time $t$ was estimated by three kinds of methods. First, the amount can be calculated using the simplest relation [13], as shown in the following equation:

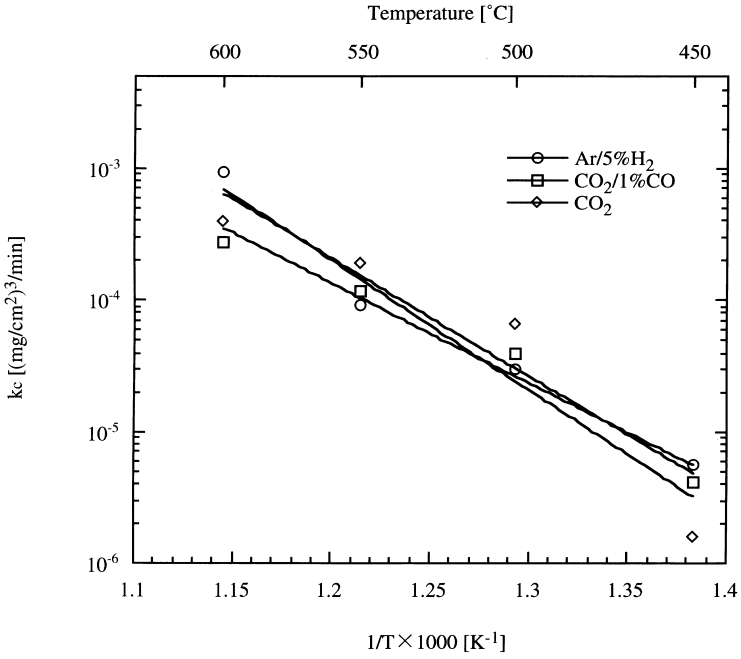


Fig. 8. The cubic rate constants as the function of reciprocal oxidation temperature.

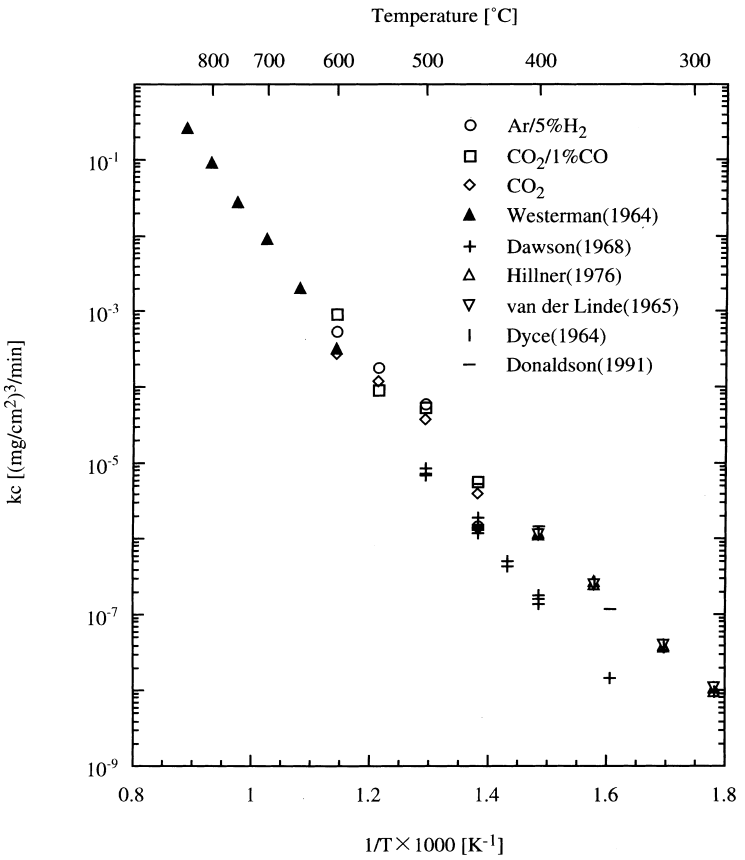


Fig. 9. The rate constants obtained in the cubic kinetic region. The rate constants of the other oxidation experiments are derived from Refs. [2–4,9].

$$M_\alpha = 2(C_s - C_o)\left(\frac{Dt}{\pi}\right)^{1/2}, \tag{6}$$

where $M_\alpha$ is the amount of oxygen in the α metallic phase, $C_s$ is the oxygen concentration in the saturated α-Zr(O), $C_o$ is the concentration of oxygen dissolved in the original specimen, and $D$ is the oxygen diffusion coefficient in α-Zr. In this study, the values used for $C_s$ and $C_o$ are 479.4 mg/cm$^3$ and 8.5 mg/cm$^3$, respectively. The diffusion coefficient is taken as $D = 0.0661\ \exp(-184\ \text{kJ/mol}/RT)\ \text{cm}^2/\text{s}$ [14]. Second, Westerman calculated $M_\alpha$ by considering the movement of the oxide/metal interface [3]. The amount of the oxygen thus obtained are comparable to the half of the amount calculated by the simplest method at less than 600°C. Third, Smith also estimated the weight of oxygen in the metal by analyzing the moving boundary problem [15]. The empirical equation is expressed as $M_\alpha = 550\ \exp(-103/RT)\sqrt{t}$. The amount of oxygen in the metal decreases with the reciprocal absolute temperature. Fig. 10 shows the effect of the dissolved oxygen on oxidation kinetics under the $CO_2$/1%CO atmosphere at 600°C. The solid line is the experimental weight gain curve under the condition mentioned above. The amount of dissolved oxygen is estimated by the three kinds of methods and then the weight of the oxide film is the solid line minus the weight of dissolved oxygen. So the oxygen dissolution into the metal under the growing oxide can alter hardly the oxidation kinetics of Zircaloy-2 at the experimental temperature range.

From the XRD examination, the peak patterns from the oxide are shown in Fig. 5(b)–(d). Monoclinic $ZrO_2$ peak pattern and tetragonal peak ($2\theta = \sim 30°$) were found in the oxidized samples. In general, $ZrO_2$ has three oxide phases; monoclinic ($T_{trs} = 1205$°C), tetragonal ($T_{trs} = 1402$°C), and cubic ($T_{trs} = 2357$°C) [1]. Here $T_{trs}$ is defined a transition temperature. In our experimental temperature range, $450\text{°C} < T < 600\text{°C}$, the oxide film seems to have only monoclinic phase from the thermodynamic data. But other researchers have reported that tetragonal phase can exist in the oxide layers [16,17]. They have explained that the tetragonal zirconia grows in the oxide layers near the metal–oxide interface where the compressive stress is very high. In this study, it

cannot be specified which position the tetragonal zirconia existed, but the existence of t-$ZrO_2$ was indicated.

In the cross-sectional photographs of the thick oxide layers, which grew under the temperature of 600°C, there were found the lateral cracks near the oxide–metal interface. Though the small cracks may exist in bulk of oxide, it is so difficult to be clearly identified. The lateral small cracks can decrease the diffusion paths of the anions [16]. The thick oxide layer is characterized by the shape of the metal–oxide interface and the place where the cracks are distributed. It is known that the oxide on the zirconium metal develops into internal matrix metal. As shown in these photographs, the metal–oxide interface shape is wavy or scalloped, resulting from the difference of the oxidation rate with positions. Two reasons were considered as the cause of this phenomenon. One is why the oxidation rate accelerates by local tensile stress, but retards by the compressive stresses in the metal. Another causes from an adherency between the oxide and the metal. If oxidation is assumed to develop at the metal–oxide interface, the cracks or voids may prevent the oxidation reaction there [17,18] because the anions are not supplied enough to the metal. The results in this study are reasonably interpreted with the latter reason.

Moreover, the character of these cracks can be related to the oxidation kinetics. The oxidation kinetics, where the rate control process is simple diffusion through the growing oxide film, obey the parabolic law. This is expressed by the following formula:

$$\frac{dW}{dt} = \frac{k_3}{W}, \tag{7}$$

where $W$ is the oxide film thickness or weight gain at time $t$. Here it is assumed that the cubic rate constant is less than the ideal parabolic one and that $k_3$ is in proportion to $1/W$. This idea is advocated by Dawson [4]. The above formula can be rewritten as

$$\frac{dW}{dt} = \frac{k_4}{W^2}. \tag{8}$$

This is the differential form of the cubic rate law. As described above, if the lateral cracks retard oxidation, these effects may reflect on the ideal parabolic rate constant $k_3$. In the case of diffusion in porous media, it is

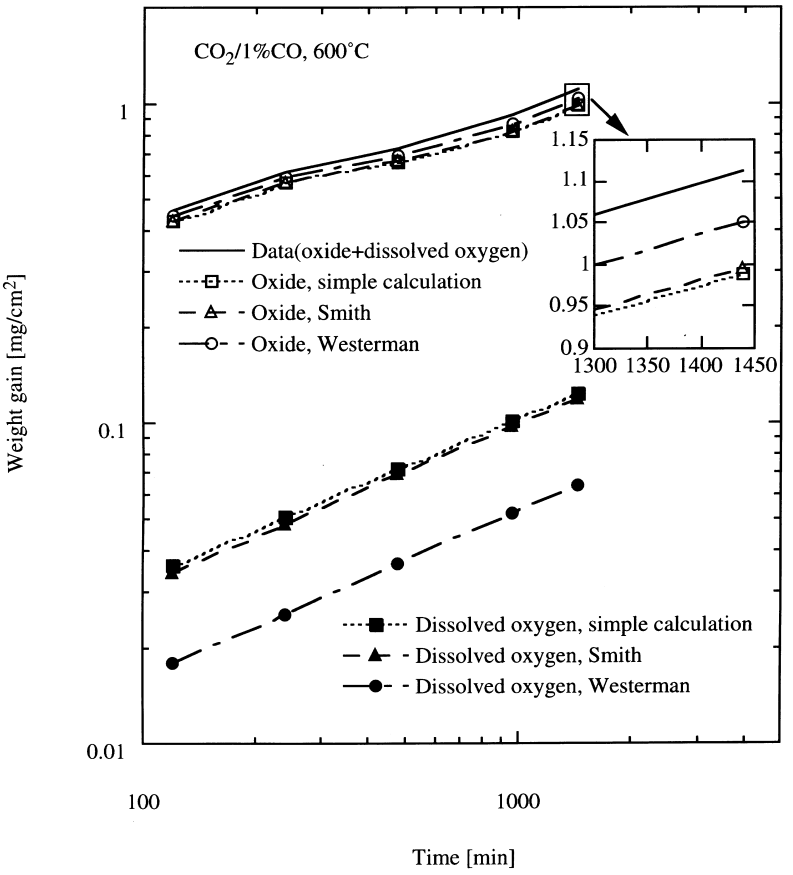


Fig. 10. The effect of the dissolved oxygen on oxidation kinetics under the $CO_2$/1%CO atmosphere at 600°C. The amount of the dissolved oxygen is estimated by the three kinds of methods: (1) simple calculation [13]; (2) by Smith [15]; (3) by Westerman [3].

known that the effective diffusion coefficient is lower than the diffusion coefficient in the absence of a porous medium because of the geometric factors, e.g., porosity, tortuosity, and constrictivity [19]. For our case, it can be imagined that the number of lateral cracks increases with thickening the oxide film so that the diffusion paths of oxygen become tortuous and an effective area, which is concerning diffusion of oxygen, can be reduced. It is, however, difficult to derive the relation between $k_3$ and $k_4$ in terms of such geometric factors mathematically. For instance, at temperature of 500°C, the relation between $k_3$, which corresponds to $W(\mathrm{d}W/\mathrm{d}t)$, and $W$ is shown in Fig. 11. The result in this figure shows that the oxidation kinetics are cubic rather than parabolic since the values of $W(\mathrm{d}W/\mathrm{d}t)$ seems to be proportional to $1/W$.

## 5. Conclusions

The oxidation kinetics of Zircaloy-2 have been studied in the temperature range of 450–600°C under the Ar/5%$H_2$, $CO_2$/1%CO, and $CO_2$ atmospheres. The weight gain due to oxidation has been measured as the function of time with the micro-balance technique.

It was found that the oxidation kinetics obeyed the cubic rate law rather than the parabolic one under the atmospheres of this study. The transition point from cubic to linear behavior could not be found in this study.

The dependence of the oxygen partial pressure on the oxidation kinetics has not been found under the present experimental conditions. This tendency can be explained by the reason why the growing zirconia may have the character to be n-type semiconductor and the diffusion process has been controlled by the anion vacancies. If there exist non-lattice diffusion processes, they can have little influence on the rate constant.

From the analysis of the temperature dependence of the oxidation rate constant, the activation energies can be obtained to be 145, 171, and 188 kJ/mol for the Ar/5%$H_2$, $CO_2$/1%CO, and $CO_2$ atmospheres, respectively. Comparing with other experimental results, it was suggested that the activation energy may have the temperature dependence. The effect of oxygen dissolution on the rate constant could not be found less than 600°C.

The X-ray diffractometry showed that the growing zirconia on Zircaloy-2 consisted mainly of monoclinic zirconia and, to a minor degree, of tetragonal one.

The cracks, which are parallel to the specimen surface and are distributed near the metal/oxide interface, are detected in the thick oxide film by the SEM examination. These lateral cracks may prevent the oxygen diffusion through the oxide film.

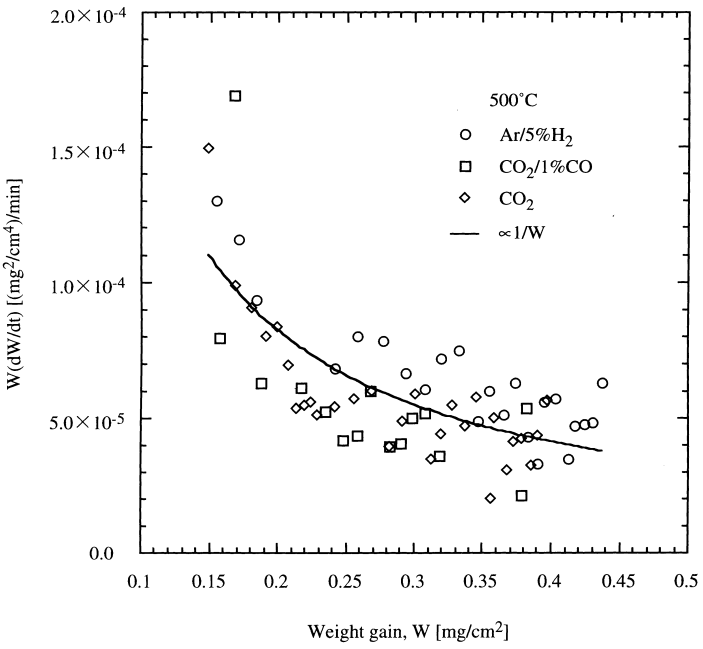


Fig. 11. $W(\mathrm{d}W/\mathrm{d}t)$ as the function of weight gain, $W$. When the oxidation kinetics obey the parabolic rate law, the values of $W(\mathrm{d}W/\mathrm{d}t)$ are constant. On the other hand, these values are proportional to $1/W$ for the cubic rate law.

## Acknowledgements

The authors gratefully acknowledge the continuous support of the technical staff, Mr M. Momoda and Mr M. Kutsuwada. We also wish to thank Dr M. Watanabe, the Center of Advanced Instrumental Analysis, Kyushu University for her help in the XRD analysis. This work was supported by a Grant-in-Aid Scientific Research from Ministry of Education, Science and Culture(No. 8780476).

## References

[1] E.H.P. Cordfunke, R.J.M. Konings, Thermochemical Data for Reactor Materials and Fission Products, North-Holland, Amsterdam, 1990.
[2] E. Hillner, in: A.L. Lowe, G.W. Parry (Eds.), Zirconium in the Nuclear Industry, ASTM-STP 633, ASTM, Philadelphia, PA, 1977, p. 211.
[3] R.E. Westerman, J. Electrochem. Soc. 111 (1964) 140.
[4] J.K. Dawson et al., J. Nucl. Mater. 25 (1968) 179.
[5] J. Nakamura et al., J. Nucl. Mater. 200 (1993) 256.
[6] R.G.J. Ball et al., J. Nucl. Mater. 167 (1989) 191.
[7] A.E. Newkirk, Anal. Chem. 32 (1960) 1558.
[8] B. Cox, J. Nucl. Mater. 218 (1995) 261.
[9] A.T. Donaldson, in: C.M. Euken, A.M. Garde (Eds.), Zirconium in the Nuclear Industry, ASTM-STP 1132, ASTM, Philadelphia, PA, 1991, p. 177.
[10] D.J. Poulton, W.W. Smeltzer, J. Electrochem. Soc. 117 (1970) 378.
[11] H.J. Beie et al., in: A.M. Garde, E.R. Bradley (Eds.), Zirconium in the Nuclear Industry, ASTM-STP 1245, ASTM, Philadelphia, PA, 1994, p. 615.
[12] B. Cox, J.P. Pemsler, J. Nucl. Mater. 28 (1968) 73.
[13] J. Crank, The Mathematics of Diffusion, Clarendon, Oxford, 1975.
[14] I.G. Richie, A. Atrens, J. Nucl. Mater. 67 (1977) 254.
[15] T. Smith, J. Electrochem. Soc. 112 (1965) 39.
[16] Y. Ding, D.O. Northwood, Corr. Sci. 36 (1994) 259.
[17] B. Hutchinson, B. Lehtinen, J. Nucl. Mater. 217 (1994) 243.
[18] J.P. Pemsler, J. Electrochem. Soc. 112 (1965) 477.
[19] J. van Brakel, P.M. Heertjes, Int. J. Heat Mass Transfer 17 (1974) 1093.